



# 1 The global database of deep-time marine nitrogen 2 isotope data

3 Yong Du<sup>1</sup>, Huyue Song<sup>1,\*</sup>, Thomas J. Algeo<sup>1,2,3,4</sup>, Hui Zhang<sup>1</sup>, Jianwei Peng<sup>1</sup>, Yuyang  
4 Wu<sup>1,5</sup>, Jiankang Lai<sup>1</sup>, Xiang Shu<sup>1</sup>, Hanchen Song<sup>1</sup>, Lai Wei<sup>6</sup>, Jincheng Zhang<sup>7</sup>, Eva E.  
5 Stüeken<sup>8</sup>, Stephen E. Grasby<sup>9</sup>, Jacopo Dal Corso<sup>1</sup>, Xiaokang Liu<sup>1</sup>, Daoliang Chu<sup>1</sup>, Li  
6 Tian<sup>1</sup>, Qingzhong Liang<sup>7</sup>, Xinchuan Li<sup>7</sup>, Hong Yao<sup>7</sup>, Haijun Song<sup>1</sup>

7 <sup>1</sup>State Key Laboratory of Geomicrobiology and Environmental Changes, School of Earth Sciences,  
8 China University of Geosciences, Wuhan 430074, China

9 <sup>2</sup>State Key Laboratory of Geological Processes and Mineral Resources, China University of  
10 Geosciences, Wuhan 430074, China

11 <sup>3</sup>Department of Geosciences, University of Cincinnati, Cincinnati, OH 45221-0013, USA

12 <sup>4</sup>State Key Laboratory of Oil and Gas Reservoir Geology and Exploitation, Chengdu University of  
13 Technology, Chengdu 610059, China

14 <sup>5</sup>College of Marine Science and Technology, China University of Geosciences, Wuhan 430074, China

15 <sup>6</sup>School of Future Technology, China University of Geosciences, Wuhan 430074, China

16 <sup>7</sup>School of Computer Science, China University of Geosciences, Wuhan 430074, China

17 <sup>8</sup>School of Earth & Environmental Sciences, University of St Andrews, St Andrews KY16 9AL, UK

18 <sup>9</sup>Geological Survey of Canada, Natural Resources Canada, Calgary, Alberta T2L 2A7, Canada

19 *Correspondence to:* Huyue Song (hysong@cug.edu.cn)

20 **Abstract.** Stable nitrogen isotope records preserved in marine sediments provide critical insights into  
21 Earth's climate history and biospheric evolution. Although numerous studies have documented nitrogen  
22 isotope ( $\delta^{15}\text{N}$ ) records across varied geological ages (Archean to Recent) and paleogeographic settings,  
23 the scientific community remains constrained by the absence of a standardized database to  
24 systematically investigate their spatiotemporal evolution. Here, we present the database of Deep-time  
25 Sediment Nitrogen Isotopes in Marine Systems (DSMS-NI), a comprehensive global compilation of  
26  $\delta^{15}\text{N}$  data and associated geochemical parameters, spanning a vast collection of sediment samples  
27 dating from the Recent to the Archean. This database encompasses 71 040  $\delta^{15}\text{N}$  records derived from  
28 424 publications, systematically organized with 29 metadata fields categories (e.g., chronostratigraphic  
29 ages, coordinates, lithology, metamorphic grade, sedimentary facies, references) encompassing 1 927  
30 829 metadata. This repository further incorporates 130 proxy data fields, including 285 715



31 geochemical data spanning total organic carbon (TOC), total nitrogen (TN), and organic carbon  
32 isotopes ( $\delta^{13}\text{C}_{\text{org}}$ ), major and trace elements and iron species. These integrated parameters enable  
33 evaluation of sample fidelity and factors influencing  $\delta^{15}\text{N}$  signatures. The DSMS-NI database will  
34 facilitate research across key geological intervals such as the Permian-Triassic boundary and the  
35 Cretaceous ocean anoxic events. Researchers can leverage temporal and paleogeographic information,  
36 alongside geochemical data, to conduct spatiotemporal analyses, thereby uncovering changes in  
37 deep-time marine nitrogen cycles and paleoenvironmental conditions. The database is open-access via  
38 the Geobiology portal (<https://geobiologydata.cug.edu.cn/>, last access: 30 April 2025), allowing users  
39 to access data and submit new entries to ensure continuous updates and expansion. This resource  
40 represents a vital foundation for studies in paleoclimate, paleoenvironment, and geochemistry, offering  
41 essential data for understanding long-term Earth-system processes. The data files described in this  
42 paper are available at <https://doi.org/10.5281/zenodo.15117375> (Du et al., 2025a)

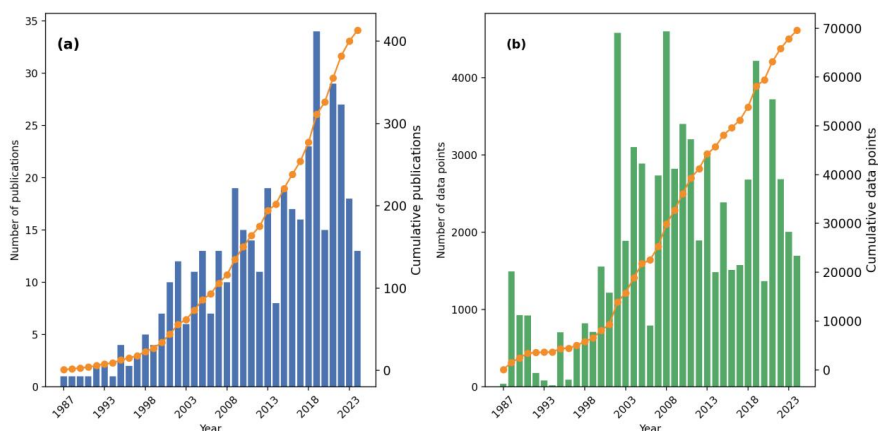
## 43 1 Introduction

44 Nitrogen, as an essential nutrient and redox-sensitive element, plays a crucial role in biological  
45 evolution and environmental climate changes (Ader et al., 2016; Pellerin et al., 2024). Typically,  
46 nitrogen isotope compositions are reported as a relative deviation of sample's isotopic ratio relative to  
47 that of atmospheric  $\text{N}_2$ , expressed in per mille (‰) as  $\delta^{15}\text{N} = (\text{R}_{\text{sample}}/\text{R}_{\text{AIR-N}_2} - 1) \times 1000$  ‰ where  $\text{R} =$   
48  $^{15}\text{N}/^{14}\text{N}$ . The  $\delta^{15}\text{N}$  record has become one of the primary tools for tracing the evolution of the nitrogen  
49 cycle and reconstructing redox conditions through deep time (Algeo et al., 2014; Sahoo et al., 2023; Du  
50 et al., 2024; Moretti et al., 2024). Advances in analytical techniques have facilitated rapid growth in the  
51 application of  $\delta^{15}\text{N}$  for paleoenvironmental studies in recent decades (Fig. 1; Zhong et al., 2023). Given  
52 nitrogen's short marine residence time of approximately 3000 years, which leads to regionally variable  
53 and rapidly shifting patterns (Gruber and Galloway, 2008), high-resolution  $\delta^{15}\text{N}$  datasets with detailed  
54 temporal and spatial coverage are critical for elucidating nitrogen cycle dynamics through Earth  
55 history.

56 Existing compilations of deep-time marine  $\delta^{15}\text{N}$  records exhibit significant limitations in term of  
57 temporal coverage and metadata compliance. Previous efforts have focused specifically on  
58 Precambrian to investigate the origins of microbial nitrogen metabolism and redox evolution during the  
59 Great Oxidation Event (Thomazo et al., 2011; Stüeken et al., 2016, 2024; Kipp et al., 2018; Uveges et  
60 al., 2025). Other studies have targeted Phanerozoic systems (Algeo et al., 2014) or specific intervals



61 such as the Paleozoic (Koehler et al., 2019), Cenozoic (Tesdal et al., 2013), Cambrian (Wang et al.,  
62 2018; Liu et al., 2020), and Triassic (Sun et al., 2024) to analyze key biological and environmental  
63 events. The largest compilation of data from pre-Cenozoic records contains fewer than 8000  $\delta^{15}\text{N}$   
64 entries, with much of the data being repetitive across different datasets (Stüeken et al., 2024). In  
65 contrast, Tesdal et al. (2013) compiled up to 33 352 entries, but all of these records are from the past 6  
66 million years. Moreover, these repositories often fail to adhere systematically to the FAIR (Findable,  
67 Accessible, Interoperable, Reusable) data principles (Wilkinson et al., 2016) and offer limited metadata  
68 categories. Typically, they provide only broad geologic ages, lithology, and metamorphic grades, while  
69 lacking essential metadata such as paleogeographic coordinates, depositional environments, and  
70 high-resolution chronostratigraphy (Table 1). Current metadata-rich databases that follow FAIR  
71 principles remain limited to fewer than 3000  $\delta^{15}\text{N}$  entries (e.g., Farrell et al., 2021; Lai et al., 2025),  
72 highlighting the urgent need for a rigorously standardized, spatiotemporally comprehensive  $\delta^{15}\text{N}$   
73 database.



74  
75 **Figure 1.** Temporal trends in (a) nitrogen isotope publications and (b)  $\delta^{15}\text{N}$  data entries in the DSMS-NI database.  
76 Vertical bars denote annual publication/dataset counts, while dots connected by lines represent cumulative totals  
77 over the years.

78  
79 The DSMS-NI database, a repository of deep-time sediment nitrogen isotopes in marine systems  
80 spanning Earth history, aims to address this need. The DSMS-NI database is a part of the broader  
81 GBDB (Geobiology Database) project, which aims to build a comprehensive database of biotic and  
82 biogeochemical evolution throughout time and to explore the mechanisms driving these evolutionary  
83 processes. By integrating detailed metadata, DSMS-NI provides a valuable resource for studying



84 nitrogen cycle evolution and paleoenvironmental conditions across a range of temporal and spatial  
 85 scales. This compilation provides an extensive survey of  $\delta^{15}\text{N}$  records for all marine sediment types,  
 86 with a particular emphasis on data predating the Cenozoic Era. Derived from 424 peer-reviewed  
 87 publications and publicly available datasets, it currently encompasses 71 040 discrete  $\delta^{15}\text{N}$   
 88 measurements for various components (e.g., bulk rock, shell-bound, kerogen). In addition, it includes  
 89 roughly 285 715 associated data points for carbon, sulfur isotopes, and major and trace element  
 90 concentrations reported alongside the  $\delta^{15}\text{N}$  values. Each entry is linked to a comprehensive set of  
 91 standardized metadata, ensuring consistency and facilitating robust data analyses. Our goal is to make  
 92 DSMS-NI a dynamic, evolving database that improves over time, with data visualizations updated  
 93 concurrently on the Geobiologydata website (<https://geobiologydata.cug.edu.cn/>, last access: 30 April  
 94 2025).

95  
 96 **Table 1** Overview of deep-time  $\delta^{15}\text{N}$  compilation.

Data Source	Number of $\delta^{15}\text{N}$ record	Metadata	Spatial range	Temporal range
Tesdal et al. (2013)	33 352	Fine age; Modern coordinate; Site	Global	Neogene to Present
Algeo et al. (2014), restricted access	6006	Broad age; Formation	Global	Ediacaran to Present
Stüeken et al. (2016)	6449	Broad age; Formation; Lithology; Metamorphic grade	Global	Since the Paleoproterozoic
Stüeken et al. (2024)	10 584	Broad age; Formation; Lithology; Metamorphic grade	Global	Since the Eoarchean
Kipp et al. (2018)	6468	Broad age; Formation; Lithology; Metamorphic grade	Global	Since the Paleoproterozoic
Koehler et al. (2019)	2454	Crude age; Formation; Lithology; Metamorphic grade	Global	Paleozoic
Farrell et al. (2021), SGP database	840	Broad age; Modern coordinate	Global	Paleozoic and Eoarchean
Lai et al. (2025), DM-SED database	2561	Fine age; Modern coordinate; Paleo-coordinate ; Site; Formation; Depositional environments;	Global	Since the Neoproterozoic



---

Lithology; Metamorphic grade

---

97

98       Version 0.0.1 of the DSMS-NI database is available in CSV format on Zenodo  
99 (<https://doi.org/10.5281/zenodo.15117375>), and dynamic updates will be maintained on the  
100 GeoBiology website. The following sections provide a comprehensive overview of the database  
101 compilation methods, data structure, and details of the dataset, including data sources, selection criteria,  
102 and definitions of metadata fields. Additionally, we analyze the temporal and spatial trends of  $\delta^{15}\text{N}$   
103 within the dataset, discuss potential applications and limitations, and outline the foundation for the  
104 database's continuous development and scientific utility.

105   **2 Compilation methods**

106   **2.1 Data compilation**

107   An extensive search was conducted based on published articles, reports, theses, and datasets to gather  
108 all available literature on deep-time nitrogen isotopes. Initially, a keyword-based search combining  
109 geological period and nitrogen isotope was performed on Google Scholar, yielding over 3000 relevant  
110 literature sources after removing duplicates. A significant portion of the articles, however, only  
111 discussed previously published  $\delta^{15}\text{N}$  data, rather than presenting newly measured data, which were  
112 manually excluded from the data compilation. Additionally, geochemical databases such as PANGAEA  
113 (<https://www.pangaea.de/>, last access: April 1 2025), EarthChem (<https://www.earthchem.org/>, last  
114 access: April 1 2025), SGP (<https://sgp-search.io/>, last access: April 1 2025), and NOAA  
115 (<https://www.ncei.noaa.gov/>, last access: April 1 2025) were queried to ensure comprehensive coverage  
116 of dataset sources (Diepenbroek et al., 2002; Gard et al., 2019; Farrell et al., 2021). Where overlaps  
117 existed between datasets and publications, journal articles were prioritized as the primary data sources.  
118 Further filtering excluded studies on non-marine sediments, entries lacking essential metadata (e.g.,  
119 geological age, latitude and longitude), and a limited number of Cenozoic records with inaccessible  
120 data. Ultimately, the curated dataset includes 424 valid sources published between 1983 and 2024,  
121 representing a comprehensive compilation of nitrogen isotope records for deep-time marine sediments.

122       Data from each publication were stored in various formats, including tables within the main text,  
123 supplementary files, or shared databases. Data extracted from tables and supplementary files were  
124 initially processed by computer algorithms, followed by manual verification and supplementation. For  
125 databases, data files were downloaded manually. In cases where publications did not provide direct



126 data, data points were extracted from figures using GetData Graph Digitizer (ver. 2.24), and these  
127 entries were labeled as "plot" in the Notes section. Each publication was then organized into an  
128 individual data file with clear labeling of sources and unique site identifiers. These files were  
129 subsequently merged into a master dataset based on standardized column headers. In the final master  
130 dataset, additional metadata were curated, including geological age, latitude and longitude, lithology,  
131 depositional facies, and metamorphic grade. High-resolution ages and paleo-coordinates were  
132 calculated and converted where applicable.

### 133 **2.2 Data selection and quality control**

134 Given that biogeochemical and paleoenvironmental studies based on nitrogen isotopes require the  
135 assessment of the depositional environment and post-depositional alteration, geochemical data apart  
136 from  $\delta^{15}\text{N}$  are crucial (Tribouvillard et al., 2006; Robinson et al., 2012). Therefore, we collected other  
137 contemporaneously published geochemical data of the same samples as  $\delta^{15}\text{N}$  from the literature  
138 relevant to the formations in our database. All available data from each research site were included as  
139 comprehensively as possible, rather than excluding entries solely due to the absence of  $\delta^{15}\text{N}$  values.  
140 This approach allows for the potential interpolation of the time-series data. However, geochemistry  
141 fields with fewer than 100 data points in the final compilation were excluded due to their limited  
142 analytical utility, such as Mo and Fe isotopes.

143 To ensure the reliability and applicability of the data, each entry underwent a rigorous screening  
144 and evaluation process. Initially, we assessed the data source and its spatiotemporal context. All studies  
145 included in the database were required to report verified  $\delta^{15}\text{N}$  values with clear data provenance and  
146 well-defined spatiotemporal information. Data entries lacking traceable sources were excluded.  
147 Similarly, entries without precise geographic or temporal information were not considered. Data from  
148 highly heterogeneous geological settings with insufficient sampling resolution were also filtered out to  
149 minimize potential biases stemming from spatial variability in lithology or metamorphic grade. For  
150 studies reporting multiple measurements across a range of water depths, depositional facies, lithologies,  
151 or fossil shells, each measurement was recorded as an independent entry. The  $\delta^{15}\text{N}$  values for bulk rock,  
152 decarbonated rock, and fossil shells were classified as primary entries, while values for other  
153 components, such as kerogen, clay-bound nitrogen, and porphyrins, were categorized solely as  
154 secondary entries. Only primary entries were analyzed in the data visualizations presented later in this  
155 study.

156 Only  $\delta^{15}\text{N}$  obtained through standardized, widely accepted techniques were included in the



157 database. These primarily consist of elemental analyzer-isotope ratio mass spectrometry methods  
158 applied to bulk rock, decarbonated fractions, or kerogen (Song et al., 2023), as well as denitrifier-based  
159 mass spectrometry methods for microfossils (Farmer et al., 2021). Studies employing non-standard or  
160 unvalidated methods, such as stepwise combustion (Ishida et al., 2017), were excluded. Data from  
161 highly metamorphosed settings (e.g., hydrothermal alteration), terrestrial lakes and rivers, modern  
162 organisms and their metabolic products, and liquid phases were flagged and omitted from the database  
163 (e.g., Bebout et al., 1999; Chase et al., 2019; Xia et al., 2022). For data from the same site but at  
164 different depths or lithologies, or for measurements of different components at the same water depth, or  
165 repeated measurements of the same sample under varying conditions, each entry was recorded  
166 separately to accurately capture variability. Statistical methods were applied to detect potential outliers  
167 in nitrogen isotope values. Isotopic values falling outside the expected range for a given geological  
168 context (e.g., extreme  $\delta^{15}\text{N}$  values in specific sedimentary rocks) were flagged for further review. If  
169 these anomalies could not be reasonably explained by contextual data, they were excluded from the  
170 final compilation.

171 Metadata on paleo-coordinates, depositional setting, lithology, and metamorphic grade are  
172 included wherever available. Entries are not excluded due to missing metadata, as these can potentially  
173 be supplemented in future research. When such metadata are not directly reported in the literature, we  
174 attempt to estimate them using supplementary data or external sources, such as paleogeographic  
175 reconstructions. For entries where metadata cannot be determined, blank values are assigned.

### 176 **3 Data summary**

177 Since nitrogen isotope studies in sediments began in the late 1980s, the number of published studies  
178 has shown an accelerating growth trend, doubling approximately every decade. This trend is mirrored  
179 by a steady increase in data volume, with an average annual addition of around 2720 data points over  
180 the past two decades (Fig. 1). However, the rate of data growth slightly lags behind that of publications,  
181 largely because early Ocean Drilling Program (ODP) and Integrated Ocean Drilling Program (IODP)  
182 projects contributed substantial datasets within individual publications (e.g., Liu et al., 2008). Ocean  
183 drilling remains a vital component of the database, covering geological intervals since the Cretaceous.  
184 Some early drilling data were not initially publicly accessible and have been supplemented through  
185 existing literature compilations, particularly the substantial dataset from Tesdal et al. (2013), along with  
186 enriched metadata.



187 The DSMS-NI database comprises a total of 29 metadata fields and 130 proxy data fields, organized  
188 into five primary categories (Table 2): (1) Sampling location, (2) Age information, (3) Geochemical  
189 data, (4) Lithological characteristics, and (5) references. For clarity and consistency throughout this  
190 data descriptor, the term "entries" refers to individual proxy values and their associated metadata (i.e.,  
191 rows), while "fields" denote the metadata attributes recorded for each entry (i.e., columns).

192

193 **Table 2** Field names and descriptions.

Field name	Description
Sample ID and location fields	
SampleID	Unique sample identification code, as originally published
SiteName	Name of the drill core site or section
SampleName	Author denoted title for the sample (often non-unique, e.g., numbered)
Location1	Detailed location of the data collection site
Location2	Country or ocean of the data collection site
Latitude	Modern latitude of collection site rounded to two decimals; negative values indicate the Southern Hemisphere (decimal degrees)
Longitude	Modern longitude of the collection site rounded to two decimals; negative values indicate the Western Hemisphere (decimal degrees)
Paleolatitude	Palaeolatitude of collection site rounded to two decimals; negative values indicate the Southern Hemisphere (decimal degrees)
Paleolongitude	Palaeolongitude of the collection site rounded to two decimals; negative values indicate the Western Hemisphere (decimal degrees)
Age fields	
Era	The geologic era, in reference to GTS v202309
Period	The geologic period, in reference to GTS v202309
Epoch	The geologic epoch, in reference to GTS v202309
Stage	The geologic stage, in reference to GTS v202309
Age	Age, in reference to GTS v202309
Formation	Geologic formation name
Unit	Specific geologic event layers
RelativeDepth	Stratigraphic height or depth (m)



Petrological characteristic fields	
Lithology	Lithological name of the sample, as originally published
LithType	Lithology type of sample (e.g., carbonate, siliciclastic)
MetamorphicGrade	The degree to which the rock has undergone transformation due to heat and pressure conditions
Setting	Depositional environment (e.g., epeiric, bathyal)
WaterDepth	Estimated depositional water depth of the data collection site
Data fields	
Isotopes	The isotope composition expressed in per mille (‰) as $\delta$ (e.g., $\delta^{15}\text{N}$ , $\delta^{13}\text{C}$ )
Elements	The concentration of elements within rocks (e.g., TN, P, Fe, Cu, Ce)
RockEval	Proxies of hydrocarbon potential measured by pyrolysis method (e.g., S1, OI, Tmax)
FeSpecies	Concentrations and ratios of different iron species in rocks (e.g., Fepy, Fehr/Fet)
Reference fields	
FirstAuthor	The last name of the first author of the original publication
Year	The year of the original publication
Title	The title of the original publication
Reference	The formatted reference of the original publication
DOI	The DOI of the original publication
DataSource	The repository hosting the data except for the original publication

194

195

196 **Sample ID and Location fields.** Each data entry is assigned a unique Sample ID to distinguish it from  
 197 other data sources. Geographic location information includes the modern latitude and longitude  
 198 (Latitude and Longitude) referencing WGS84 (World Geodetic System 1984), obtained directly from  
 199 original literature or external sources whenever possible. For studies that do not provide exact  
 200 coordinates, approximate locations are estimated based on geographic descriptions or accompanying  
 201 maps, using tools such as Google Maps. Additionally, we record the broader sampling region (e.g.,  
 202 country or oceanic region) and specific sampling site details (such as province, county, or uplift names).  
 203 The location fields also include the name of the drilling site or outcrop section (SiteName), which



204 identifies the precise drilling location or outcrop where samples were collected, providing valuable  
205 geographic context. Certain SiteNames are uniquely associated with major drilling projects (e.g., ODP,  
206 IODP), which is important for subsequent data supplementation and analysis. Some samples also have  
207 a SampleName, as designated by the original authors—typically a code or non-unique label reflecting  
208 the naming format in the primary literature. Although multiple samples in the database may share the  
209 same SampleName, each entry has a distinct Sample ID to ensure uniqueness across records.

210 We also provide paleolatitude and paleolongitude (PaleoLatitude and PaleoLongitude), calculated  
211 based on the geological age of each sample and using paleogeographic reconstruction tools such as  
212 PointTracker v7.0, built on the plate rotation model of Scotese and Wright (2018). Paleo-coordinate  
213 data are crucial for understanding the historical shifts in sample locations and their relationship to  
214 depositional environments (Percival et al., 2022; Li et al., 2025). To maintain consistency, all  
215 geographic coordinates are standardized to two decimal places.

216 **Age fields.** Each entry includes not only absolute age data but also a series of geologic age-related  
217 fields to provide precise temporal context. These fields enable targeted data retrieval across different  
218 geological time frames, facilitating comparisons with newly added data. The GeologicalAge field  
219 captures broad temporal frameworks, recorded as Epoch for the Phanerozoic (e.g., Early Triassic) and  
220 Era for the Precambrian (e.g., Neoproterozoic). For more refined stratigraphic resolution, the Stage  
221 field (e.g., Induan) is used, with the System as a substitute for Precambrian samples (e.g., Ediacaran).  
222 The Age field records the absolute age of each sample, following the International Chronostratigraphic  
223 Chart, GTS v202309. The Formation field notes the geological unit (formation or member) from which  
224 the sample was collected, aiding in understanding its depositional context and relation to surrounding  
225 strata (Murphy and Salvador, 1999). However, Formation data are generally limited to outcrop sections,  
226 as ocean drilling samples lack specific formation designations. The Unit field identifies particular  
227 stratigraphic units or geologic event layers, such as the Cretaceous pre-OAE2 or OAE2 (Jenkyns,  
228 2010), which aids in correlating samples across recognized geological events. The RelativeDepth field  
229 records the sample's relative depth in the section or drill core, which is essential for high-resolution age  
230 analyses and sedimentation rate calculations.

231 Age data allocation follows these guidelines: when precise ages and geological age information  
232 for each sample were provided in the original source, these values are prioritized. For older studies  
233 with time boundaries that do not align with the GTS v202309 of the International Chronostratigraphic  
234 Chart, boundaries are adjusted to the latest standards. If exact ages are unavailable for all samples but



235 can be determined for two or more samples or layers, an age-depth model is constructed based on  
236 RelativeDepth to estimate the ages of individual samples. For samples with only one age constraint, the  
237 median age of the corresponding geologic interval is assigned.

238 **Data fields.** The dataset includes analyses of isotopic compositions, elemental concentrations, and  
239 specific components. To maintain consistency, all units were standardized during data collection, as  
240 original publications sometimes report these data in varying units. (1) Isotopic data include  $\delta^{15}\text{N}$ ,  $\delta^{13}\text{C}$ ,  
241  $\delta^{18}\text{O}$ , and  $\delta^{34}\text{S}$ , all expressed in ‰ relative to international standards. Nitrogen isotopes are reported  
242 relative to atmospheric nitrogen (Air  $\text{N}_2$ ), carbon and oxygen isotopes relative to the Vienna Pee Dee  
243 Belemnite (VPDB) standard, and sulfur isotopes relative to the Vienna Canyon Diablo Troilite (VCDT)  
244 standard (Hoefs, 2009). (2) Elemental concentrations include TN (Total Nitrogen), TOC (Total Organic  
245 Carbon), TS (Total Sulfur),  $\text{CaCO}_3$ , TC (Total Carbon), TIC (Total Inorganic Carbon), P, Al, K, Si, Ca,  
246 Ti, Na, Mg, Fe, as well as iron species data and LOI (Loss on Ignition), and they are reported in weight  
247 percent (wt %). Concentrations of other trace elements are standardized to parts per million (ppm). (3)  
248 Some data originally reported as oxide concentrations were converted to elemental concentrations  
249 based on stoichiometric ratios, such as  $\text{P}_2\text{O}_5$ . (4) Additional derived values include ratios of iron species,  
250 dry bulk density, and rock eval indices (Peters et al., 1986; Poulton and Canfield, 2005). These indices  
251 comprise Alkenone Content (C37, in nmol/g), Oxygen Index (OI, mg  $\text{CO}_2$ /g TOC), Hydrogen Index  
252 (HI, mg HC/g TOC), maximum pyrolysis temperature ( $T_{\text{max}}$ , °C), free hydrocarbons (S1, mg HC/g  
253 Rock), hydrocarbons generated from rock pyrolysis (S2, mg HC/g Rock), and  $\text{CO}_2$  released from  
254 organic matter pyrolysis (S3, mg  $\text{CO}_2$ /g Rock). Some inaccessible data points were visually extracted  
255 from figures using scatterplot recognition techniques, which are marked as "plot" in the Note field.  
256 Data with values exceeding detection limits or those erroneous (e.g., negative values for element  
257 concentration) were excluded from the dataset.

258 **Petrological characteristic field.** The petrological characteristic fields encompass information on  
259 lithology, depositional facies, and metamorphic grade, which provide essential contextual support for  
260 subsequent isotopic geochemistry analyses. (1) Lithology: The Lithology field records the original  
261 descriptions provided by authors, using terms such as "black shale" "mudstone" "limestone" and  
262 "breccia". The LithType field classifies these lithologies into broader categories, primarily as carbonate  
263 and siliciclastic (Tucker and Wright, 2009), with minor entries for phosphorite and iron formations. (2)  
264 Metamorphic grade: The metamorphic grade field reflects the extent of metamorphism the samples  
265 have undergone, based on original terminology whenever possible. Common terms include specific



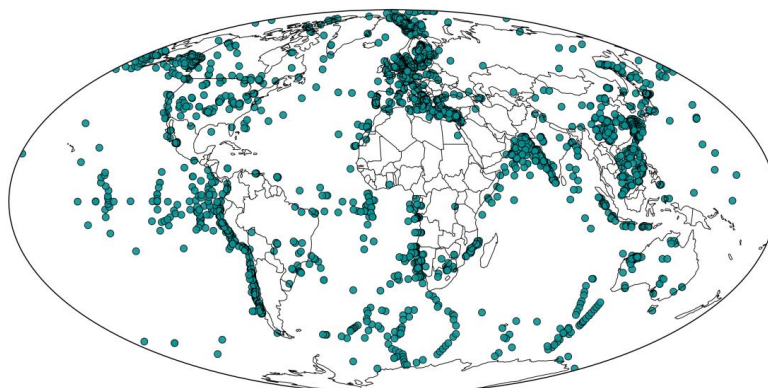
266 metamorphic facies (e.g., amphibolite, greenschist) as well as general descriptors like  
267 "unmetamorphosed" and "low grade". For Cenozoic samples, which are generally assumed to have  
268 undergone minimal metamorphic alteration (Winter, 2014), any entries lacking detailed descriptions are  
269 uniformly designated as "unmetamorphosed". (3) Depositional setting: This field records the  
270 depositional environment of each sample, with terms like "neritic" "peritidal" "slope" and "abyssal"  
271 preserved from the original literature. For many ocean drilling samples, depositional settings are  
272 inferred from WaterDepth: depths of 500–2000 m are classified as "bathyal" and depths exceeding  
273 2000 m are designated as "abyssal" ().

274 **Data collection sources.** Data in the database primarily originate from published literature and are  
275 traceable via DOI. Some data come from public databases such as PANGAEA, SGP, and NOAA. Each  
276 record includes multiple fields for source information, such as first author, publication year, article title,  
277 reference, DOI, and data source. Metadata fields have been standardized and cleaned via code to ensure  
278 consistency and machine readability, removing special characters while retaining complete citation  
279 formats. This structure allows users to trace data provenance, with DOI or Reference fields facilitating  
280 direct searches on Crossref for verification.

#### 281 **4 Technical validation**

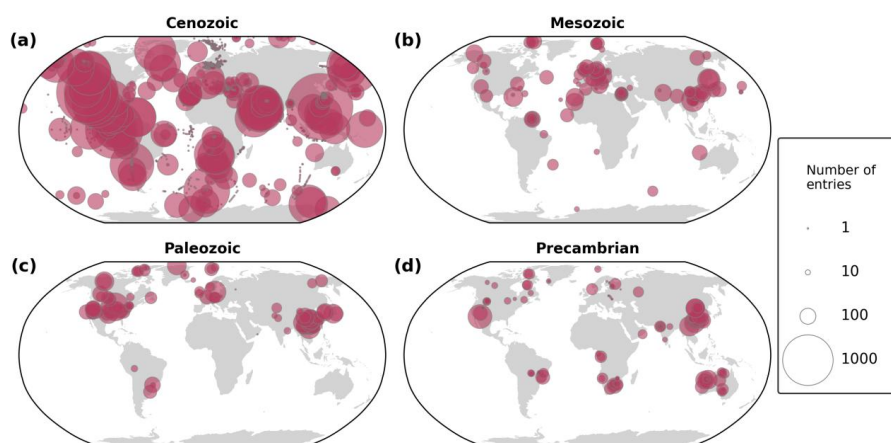
282 The DSMS-NI database has undergone meticulous curation and quality control (QC) to ensure data  
283 accuracy, consistency, and scientific value. Each record includes comprehensive metadata to support  
284 traceability and verification. While each entry and significant metadata contain a simple remarks field  
285 (excluded from the main database to prevent clutter), it notes the source or reason for inclusion,  
286 facilitating validation and cross-checking by the data management team. We implemented several QC  
287 measures to verify database accuracy.

288 Geographic coordinate verification. Latitude and longitude values were checked to confirm they  
289 fall within the valid ranges of -90 to 90 and -180 to 180, respectively. Sample coordinates were  
290 cross-referenced with country names and public national boundaries to ensure geographic accuracy.  
291 Modern sample coordinates were projected onto a global map with administrative boundaries (Figs. 2-3)  
292 to verify logical placements. If coordinates appeared on land or in other unexpected locations, each  
293 entry was manually reviewed and corrected as needed.



294

295 **Figure 2.** Distribution of sample sites on modern global map.



296

297 **Figure 3.** Spatial distribution of sampling sites and sample quantities by geological era in a modern geographic  
298 reference frame. The base map is adapted from Kocsis and Scotese (2021). The term "entries" refers to individual  
299 proxy values and their associated metadata (i.e., rows in the DSMS-NI database).

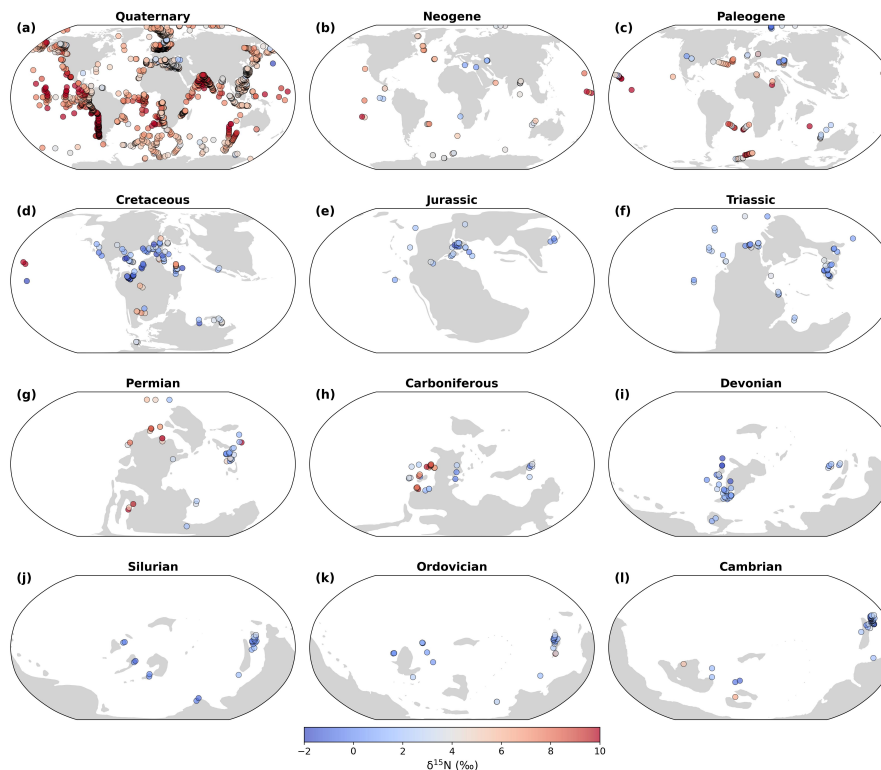
300

301 Paleocoordinate validation. Paleolatitudes and paleolongitudes were calculated using the G-Plates  
302 model (Scotese and Wright, 2018) and PointTracker v7.0 software, ensuring alignment with each  
303 sample's geological age and geographical context. Site locations were plotted on paleogeographic maps  
304 (Fig. 4) for further evaluation; any inconsistencies in paleocoordinates were flagged, reviewed, and  
305 adjusted accordingly.

306 Outlier detection. Frequency histograms and time-series scatter plots were generated to identify  
307 potential outliers in the dataset. Any extremely high or low values underwent secondary validation to  
308 confirm their accuracy. For instance, unusually high or low  $\delta^{15}\text{N}$  values were rigorously checked



309 against the original sources to verify the analytical methods and sample characteristics.



310

311 **Figure 4.** Paleogeographic distribution of  $\delta^{15}\text{N}$  values by geological period. The base map is adapted from Kocsis  
312 and Scotese (2021).

313

314 Duplicate check. We conducted a comprehensive check for duplicate entries, especially for  
315 samples with similar GPS coordinates. All suspected duplicates were carefully compared, and  
316 necessary corrections were made to eliminate redundancy.

317 Age model calibration. For cases where geological time boundaries in older publications did not  
318 align with current standards, we calibrated these boundaries according to the latest Geological Time  
319 Scale (GTS v202309). For samples lacking precise ages, an age-depth model was constructed based on  
320 RelativeDepth information provided in the literature, allowing for high-resolution age estimation of  
321 individual samples. In instances where only a single known age was available for a sample point, the  
322 median age of the corresponding geological interval was assigned. To minimize errors, geological age  
323 data were entered using a standardized template to prevent typos, inconsistencies, or incorrect values.  
324 Automated analyses and cross-verification ensured that numerical ages corresponded accurately with  
325 designated eras and geological stages.



326 Data collection sources. Citation information within the reference field was obtained through  
 327 automated methods from the CrossRef platform, ensuring uniformity in citation formatting (Hendricks  
 328 et al., 2020). We used scripts to extract comprehensive bibliographic details for each publication,  
 329 including author names, title, publication year, journal name, volume, page numbers, and DOI. This  
 330 automation significantly reduced potential spelling errors and inconsistencies that may arise in manual  
 331 entry. Extracted citation data were cross-checked against original entries in the database, and any  
 332 discrepancies or errors were corrected manually by the data management team to maintain source  
 333 accuracy and completeness.

### 334 5 General database statistics

335 The latest version of the DSMS-NI database comprises approximately 320,000 data entries, including  
 336 71 040  $\delta^{15}\text{N}$  records, spanning all geological periods from the Eoarchean (~3800 Ma) onward. These  
 337 records originate from a diverse array of unique sampling sites, encompassing ocean drilling cores and  
 338 outcrop sections. The  $\delta^{15}\text{N}$  data are predominantly concentrated in the Phanerozoic, comprising 92.1 %  
 339 of the total database, with further breakdowns showing 71.6 % in the Cenozoic, 8.3 % in the Mesozoic,  
 340 and 12.2 % in the Paleozoic (Table 3 and Fig. 3). The following sections focus on first-order spatial and  
 341 temporal trends in  $\delta^{15}\text{N}$  data density, sampling locations, and values within DSMS-NI. The provided  
 342 figures illustrate only a subset of the spatial-temporal patterns uniquely revealed by this extensive  
 343 compilation, demonstrating the database's potential to advance research in paleoclimate, geochemistry,  
 344 and paleoecology.

345

346 **Table 3** The quantities and proportions for  $\delta^{15}\text{N}$ ,  $\delta^{13}\text{C}_{\text{org}}$ , TN, and TOC of each geological era.

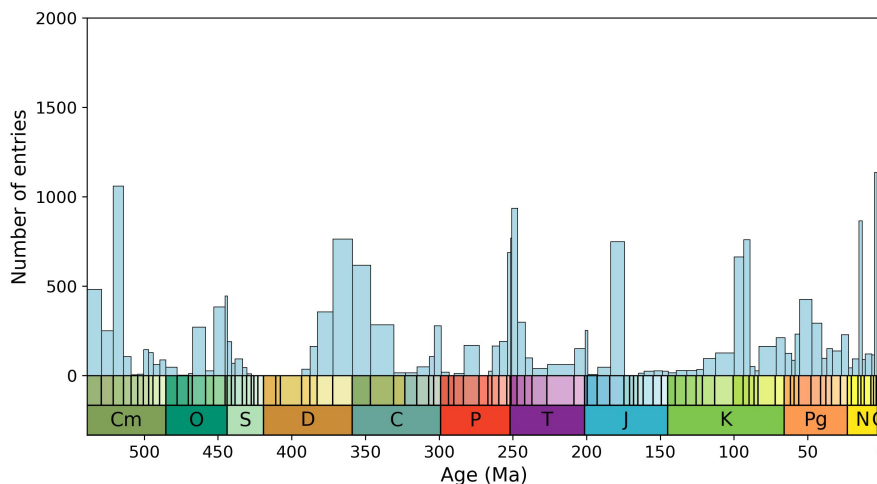
Proxy system	Cenozoic	Mesozoic	Paleozoic	Precambrian	Total
$\delta^{15}\text{N}$	50847	5894	8653	5646	71040
	71.6 %	8.3 %	12.2 %	7.9 %	
$\delta^{13}\text{C}_{\text{org}}$	10781	4902	6856	4493	27032
	40.0 %	18.1 %	25.4 %	16.6 %	
TN	31576	2855	6473	4942	45846
	68.9 %	6.2 %	14.1 %	10.8 %	
TOC	22613	5075	8597	5150	41435
	54.6 %	12.2 %	20.7 %	12.4 %	



347

### 348 5.1 Temporal density and evolution of $\delta^{15}\text{N}$

349 Given that the data are concentrated in the Phanerozoic, where ages are more precisely constrained, we  
350 performed a detailed stratigraphic breakdown of age distribution by stage within the Phanerozoic (Fig.  
351 5). The distribution is uneven, with the highest data densities in recent periods, particularly the  
352 Holocene (0-12 ka), Late Pleistocene (12-129 ka), and Chibanian (129-770 ka). The high data density  
353 in the Quaternary primarily reflects the abundance of high-resolution records from ocean drilling  
354 projects, where individual cores contribute extensive and densely sampled datasets. In contrast, older  
355 geological periods exhibit data clusters around key events, such as biotic radiations, mass extinctions,  
356 and oceanic anoxic events (Bush and Payne, 2021). Notable gaps or low-density intervals occur from  
357 the mid-Cambrian to Early Ordovician, Silurian to Early Devonian, mid-Carboniferous to Early  
358 Permian, mid-Triassic to Early Jurassic, and Late Jurassic to Early Cretaceous.



359

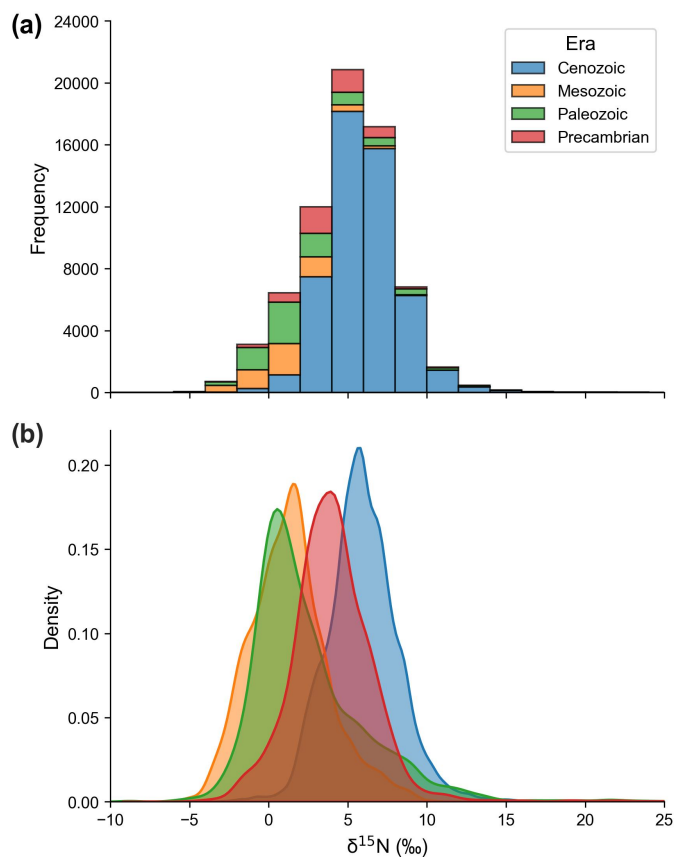
360 **Figure 5.** Number of data points binned by geologic stage. Data counts for the Holocene (0-12 ka), Late  
361 Pleistocene (12-129 ka), and Chibanian (129-770 ka) stages are 10 640, 21 754, and 8378, respectively; these  
362 counts are not displayed in the figure due to narrow column width. The Precambrian has only 5646 data points,  
363 accounting for 7.9%, and is not plotted. Cm: Cambrian; O: Ordovician; S: Silurian; D: Devonian; C: Carboniferous;  
364 P: Permian; T: Triassic; J: Jurassic; K: Cretaceous; Pg: Paleogene; N: Neogene; Q: Quaternary.

365

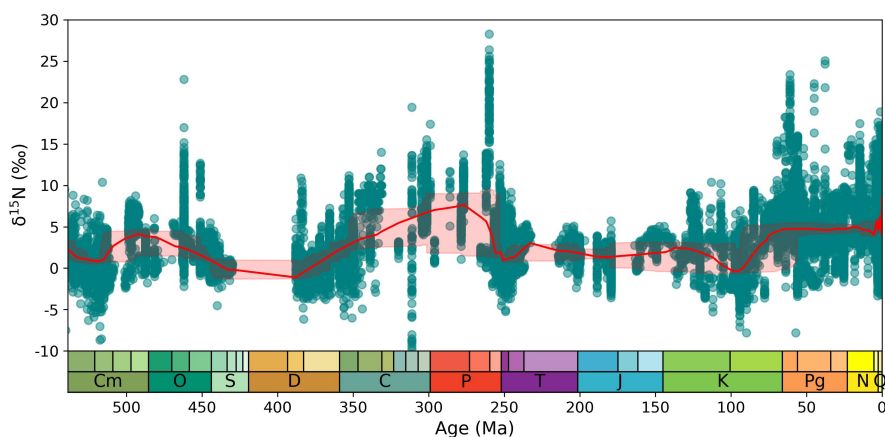
366 Overall,  $\delta^{15}\text{N}$  values exhibit a unimodal distribution centered around +5 ‰, with a mean of  $5.1 \pm$   
367  $9.1 \text{ ‰}$  ( $1\sigma$ ; Fig. 6a). Examining data density by era, the Cenozoic has the highest overall peak,  
368 followed by the Precambrian, with lower peaks in the Paleozoic and Mesozoic (Fig. 6b). Plotting all



369  $\delta^{15}\text{N}$  data on the Phanerozoic geological timescales reveals notable peaks in the Late Cretaceous,  
370 Carboniferous-Permian, mid-Triassic, Jurassic, and Early Cretaceous, which align with  
371 greenhouse-icehouse climate cycles (Fig. 7; Algeo et al., 2014). In the Precambrian, data distribution is  
372 more dispersed, potentially reflecting the instability of the nitrogen cycle or the influence of stronger  
373 metamorphic overprints (Fig. 8; Ader et al., 2016; Stüeken et al., 2024). Despite differences in  
374 paleolatitude, shifts in  $\delta^{15}\text{N}$  exhibit consistent directional changes (increase or decrease) during key  
375 Phanerozoic transition events, such as the Permian-Triassic boundary (Knies et al., 2013; Du et al.,  
376 2021, 2023) and the Late Cretaceous (Meyers et al., 2009; Junium et al., 2018; Du et al., 2025b).  
377 LOWESS smoothing results reveal  $\delta^{15}\text{N}$  peaks in the Neoproterozoic, Paleoproterozoic, and Ediacaran, i.e.,  
378 periods closely associated with significant oxygenation events (Kipp et al., 2018; Koehler et al., 2019;  
379 Pellerin et al., 2024). These temporal patterns underscore the role of nitrogen isotopes in tracing the  
380 interplay between nitrogen cycling and shifts in Earth's oxygenation history.

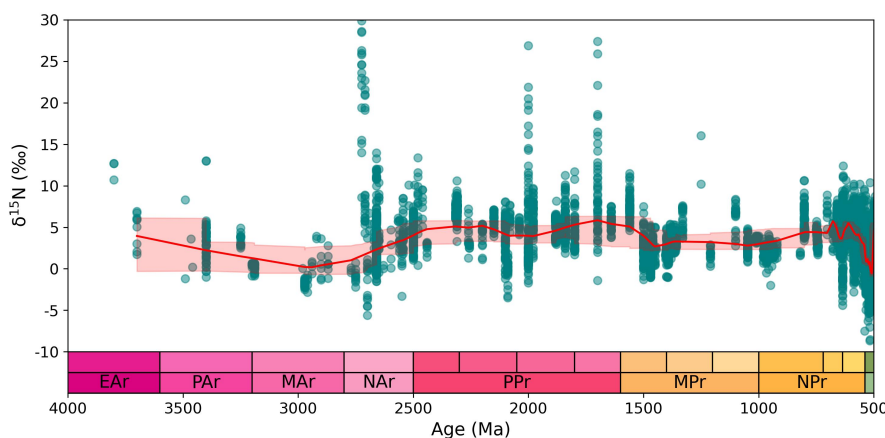


381  
382 **Figure 6.** (a) Histogram and (b) density distribution of all  $\delta^{15}\text{N}$  data.



383

384 **Figure 7.**  $\delta^{15}\text{N}$  data and LOWESS curve through Phanerozoic. A LOWESS factor of 0.03 and a confidence interval  
385 of 2.5–97.5 % were applied.



386

387 **Figure 8.**  $\delta^{15}\text{N}$  data and LOWESS curve through Precambrian. A LOWESS factor of 0.01 and a confidence  
388 interval of 2.5–97.5 % were applied. EAr: Eoarchean; PAr: Paleoarchean; MAr: Mesoarchean; NAr: Neoproterozoic;  
389 PPr: Paleoproterozoic; MPr: Mesoproterozoic; NPr: Neoproterozoic.

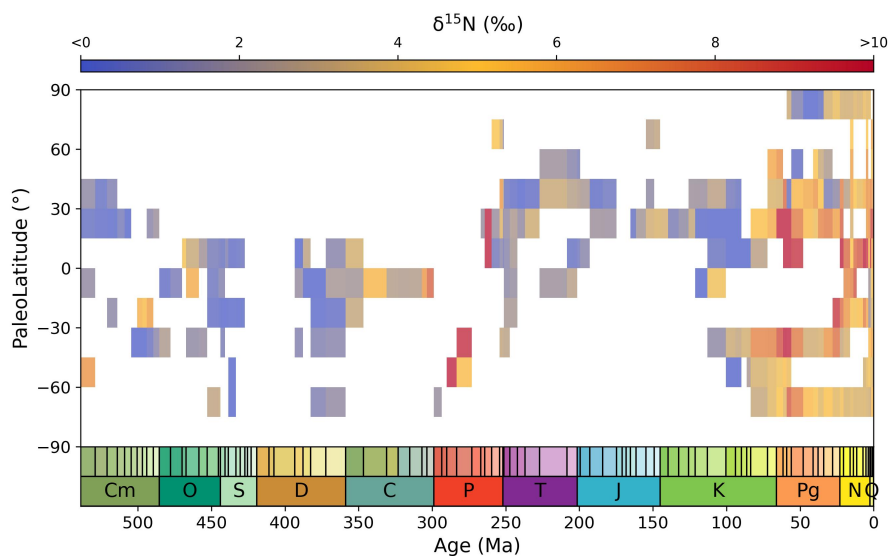
390

## 391 5.2 Spatial density and characteristics of $\delta^{15}\text{N}$

392 Spatial trends in data density across the DSMS-NI database reveal substantial variability in both  
393 modern (Fig. 2) and paleogeographic distributions (Fig. 4). Ocean drilling sites are primarily  
394 concentrated along continental margins and deep-sea basins, with significant gaps in central oceanic  
395 regions (National Research Council, 2011). For older strata (pre-Cretaceous), sampling sites are  
396 clustered in North America, Europe, China, and South Africa (Fig. 2). In terms of latitude,  $\delta^{15}\text{N}$



397 sampling in older strata is sparse in the modern equatorial region and the mid- to high-latitude areas of  
398 the Southern Hemisphere, aside from some Southern Hemisphere samples collected from Cenozoic  
399 ocean drilling sites (Fig. 3). When modern coordinates are converted to paleolatitudes and mapped onto  
400 paleogeographic reconstructions, the Quaternary shows the highest number of sites, followed by the  
401 Cretaceous. Only Cenozoic sites provide extensive latitudinal coverage (Fig. 9). In terms of marine  
402 spatial distribution,  $\delta^{15}\text{N}$  data since the Cretaceous reflects global patterns to a certain degree (Fig. 4).  
403 However, pre-Jurassic data remain spatially concentrated, with Paleozoic sites limited to just two or  
404 three main areas. High-latitude sampling is generally scarce, with Paleozoic sites predominantly in the  
405 Southern Hemisphere and Mesozoic sites mainly in the Northern Hemisphere (Fig. 4).



406  
407 **Figure 9.** Spatio-temporal trends in  $\delta^{15}\text{N}$  values through Phanerozoic, binned and averaged temporally by stage  
408 and spatially by  $15^\circ$  paleolatitudinal bins.

409  
410 Significant spatial differences exist in  $\delta^{15}\text{N}$  distribution across geological periods. Only a few  
411 periods allow for robust assessments of latitudinal gradients. For example, Cenozoic  $\delta^{15}\text{N}$  values tend  
412 to decrease with increasing latitude globally, while Ediacaran  $\delta^{15}\text{N}$  values exhibit the opposite trend  
413 (Fig. 9). To visualize spatial trends, average  $\delta^{15}\text{N}$  values from each Phanerozoic period were mapped  
414 onto paleogeographic reconstructions for the respective period (Fig. 4). Quaternary records show the  
415 highest  $\delta^{15}\text{N}$  values in areas associated with upwelling, such as the Arabian Sea, southeastern Indian  
416 Ocean, eastern equatorial Pacific, southwestern South America, and the western coast of Mexico (Fig.  
417 4a; Altabet et al., 1999; Tesdal et al., 2013). For the Paleogene and Neogene,  $\delta^{15}\text{N}$  hotspots are



418 generally located in deep-sea regions, potentially representing more positive  $\delta^{15}\text{N}$  averages across  
419 ocean basins (Fig. 4b-c). In the Paleozoic and Mesozoic,  $\delta^{15}\text{N}$  values are generally negative, lacking  
420 prominent hotspots except in the Carboniferous and Permian. Some periods exhibit slight trends of  
421 lower values at low latitudes and higher values at high latitudes, as well as more positive  $\delta^{15}\text{N}$  values  
422 near coastlines compared to more distal marine settings (Fig. 4d-l). These observations suggest that  
423 increased temporal resolution is needed for in-depth analysis of spatial  $\delta^{15}\text{N}$  variations. Given the  
424 current uneven distribution of sampling sites, further  $\delta^{15}\text{N}$  studies across diverse regions are crucial for  
425 enhancing our understanding of the spatial characteristics of nitrogen cycle evolution.

## 426 **6 Usage notes**

### 427 **6.1 Informed user notice**

428 Each record (row) in the database includes detailed temporal and spatial metadata, along with lithology,  
429 metamorphic grade, and depositional facies information where available. These metadata are essential  
430 for evaluating the geological context and fidelity of nitrogen isotope data. However, this version of the  
431 database has certain limitations; for instance, it may not capture all possible geological age  
432 uncertainties or precise depositional environment details for some records. Despite our extensive  
433 efforts to accurately identify and quality-control each entry, given the vast dataset, some overlooked  
434 errors or data inconsistencies may remain. Users are encouraged to report any issues or omissions to  
435 the authors, as corrections will be incorporated into future database versions. We recommend that users  
436 carefully review metadata fields to ensure that the data aligns with their research needs.

437 In addition to  $\delta^{15}\text{N}$  data, the database provides geochemical information such as TOC, total TN,  
438  $\delta^{13}\text{C}_{\text{org}}$ , and major and trace element concentrations. These supplementary data are valuable for  
439 assessing factors that may influence nitrogen isotopes, such as organic matter preservation and redox  
440 conditions. Even when not directly paired with  $\delta^{15}\text{N}$  values, we retain all relevant data to enable users  
441 to conduct correlation analyses via interpolation or other methods. Researchers are welcome to  
442 contribute additional geochemical data from the same sites or samples as they become available,  
443 allowing for updates and refinements in subsequent database releases.

### 444 **6.2 Applying the database in deep time**

445 When applying the database to deep-time studies, certain filtering criteria can be used. For instance,  
446 samples may be selected based on lithology, metamorphic grade, and other metadata to ensure that the



447 data aligns with specific geological research contexts. Temporal, paleolatitude, and paleodepth  
448 information are critical for paleogeographic reconstructions and spatiotemporal distribution analyses,  
449 particularly when investigating paleoclimate change and global biogeochemical cycles. Further  
450 analysis of variations in latitude, basin characteristics, and water depth has the potential to yield  
451 significant insights. Given the rapid variability of nitrogen isotopes and their pronounced regional  
452 characteristics, filling temporal and spatial gaps and enhancing resolution are of great  
453 value—particularly for pivotal periods like the Ordovician-Silurian mass extinction, the Early  
454 Devonian terrestrial plant radiation, and the Late Jurassic-Early Cretaceous supercontinent breakup.  
455 The database is also especially suited for comparative studies of key geological periods, such as the  
456 Permian-Triassic boundary extinction and the Cretaceous OAE2. To support these applications, we  
457 have also provided a software tool on Zenodo, allowing users to generate heatmaps of  $\delta^{15}\text{N}$  data  
458 distributions for specific time intervals. These heatmaps visualize the average spatial distribution of  
459  $\delta^{15}\text{N}$  for any selected geological interval, offering preliminary validation for user hypotheses and aiding  
460 in uncovering the evolution of the global nitrogen cycle.

#### 461 **7 Data availability**

462 The DSMS-NI version 0.0.1 can be accessed via Zenodo at <https://doi.org/10.5281/zenodo.15117375>  
463 (Du et al., 2025a) and via the GeoBiology website at <https://geobiologydata.cug.edu.cn/> (last access:  
464 April 30 2025).

#### 465 **8 Code availability**

466 The code used to validate the dataset and make the figures in this manuscript is available on Zenodo  
467 (<https://doi.org/10.5281/zenodo.15758073>). The paleocoordinates were estimated using the  
468 PointTracker v7 tool published by the PALEOMAP Project, which can be found at  
469 <http://www.paleogis.com> (last access: April 1 2025; <https://doi.org/10.13140/RG.2.1.2011.4162>,  
470 Scotese, 2008).

471 **Author contributions.** YD, HYS and HJS designed the study and secured funding. TJA, EES, SEG,  
472 JDC, YD, HZ, XKL, JP, YW, JK, XS, HS, DC and LT conducted data acquisition, curation and  
473 validation. YD, LW, JZ, QL, XCL and HY developed computational methodologies and provided  
474 technical support. YD prepared the paper with contribution from all co-authors.



475 **Competing interests.** The authors declare that they have no conflicts of interest.

476 **Acknowledgements.** This work has benefited from previous  $\delta^{15}\text{N}$  datasets compiled by Jan-Erik Tesdal,  
477 Christophe Thomazo, Thomas J. Algeo, Eva E. Stüeken, Magali Ader, Xinqiang Wang, and Michael A.  
478 Kipp.

479 **Financial support.** This work has been funded by the State Key R&D Project of China  
480 (2023YFF0804000), the National Natural Science Foundation of China (42172032; 42325202;  
481 42402316), the Postdoctoral Fellowship Program of CPSF (GZB20230679), the Postdoctor Project of  
482 Hubei Province (2024HBBHCXB087), the Natural Science Foundation of Hubei Province  
483 (2023AFA006).

#### 484 **References**

485 Ader, M., Thomazo, C., Sansjofre, P., Busigny, V., Papineau, D., Laffont, R., Cartigny, P., and  
486 Halverson, G. P.: Interpretation of the nitrogen isotopic composition of Precambrian sedimentary  
487 rocks: Assumptions and perspectives, *Chem. Geol.*, 429, 93–110,  
488 <https://doi.org/10.1016/j.chemgeo.2016.02.010>, 2016.

489 Algeo, T. J., Meyers, P. A., Robinson, R. S., Rowe, H., and Jiang, G. Q.: Icehouse–greenhouse  
490 variations in marine denitrification, *Biogeosciences*, 11, 1273–1295,  
491 <https://doi.org/10.5194/bg-11-1273-2014>, 2014.

492 Altabet, M. A., Murray, D. W., and Prell, W. L.: Climatically linked oscillations in Arabian Sea  
493 denitrification over the past 1 m.y.: Implications for the marine N cycle, *Paleoceanography*, 14,  
494 732–743, <https://doi.org/10.1029/1999PA900035>, 1999.

495 Bebout, G. E., Cooper, D. C., Bradley, A. D., and Sadofsky, S. J.: Nitrogen-isotope record of fluid-rock  
496 interactions in the Skiddaw aureole and granite, English Lake District, *Am. Mineral.*, 84,  
497 1495–1505, <https://doi.org/10.2138/am-1999-1002>, 1999.

498 Bush, A. M. and Payne, J. L.: Biotic and Abiotic Controls on the Phanerozoic History of Marine  
499 Animal Biodiversity, *Annu. Rev. Ecol. Evol. Syst.*, 52, 269–289,  
500 <https://doi.org/10.1146/annurev-ecolsys-012021-035131>, 2021.

501 Chase, B. M., Niedermeyer, E. M., Boom, A., Carr, A. S., Chevalier, M., He, F., Meadows, M. E., Ogle,  
502 N., and Reimer, P. J.: Orbital controls on Namib Desert hydroclimate over the past 50,000 years,



- 503 Geology, 47, 867–871, <https://doi.org/10.1130/G46334.1>, 2019.
- 504 Diepenbroek, M., Grobe, H., Reinke, M., Schindler, U., Schlitzer, R., Sieger, R., and Wefer, G.:  
505 PANGAEA—an information system for environmental sciences, *Comput. Geosci.*, 28, 1201–1210,  
506 [https://doi.org/10.1016/S0098-3004\(02\)00039-0](https://doi.org/10.1016/S0098-3004(02)00039-0), 2002.
- 507 Du, Y., Song, H., Tong, J., Algeo, T. J., Li, Z., Song, H., and Huang, J.: Changes in productivity  
508 associated with algal-microbial shifts during the Early Triassic recovery of marine ecosystems,  
509 *Geol. Soc. Am. Bull.*, 133, 362–378, <https://doi.org/10.1130/B35510.1>, 2021.
- 510 Du, Y., Song, H., Grasby, S. E., Xing, T., Song, H., Tian, L., Chu, D., Wu, Y., Dal Corso, J., Algeo, T. J.,  
511 and Tong, J.: Recovery from persistent nutrient-N limitation following the Permian–Triassic mass  
512 extinction, *Earth Planet. Sci. Lett.*, 602, 117944, <https://doi.org/10.1016/j.epsl.2022.117944>, 2023.
- 513 Du, Y., Song, H., Stüeken, E. E., Grasby, S. E., Song, H., Tian, L., Chu, D., Dal Corso, J., Li, Z., and  
514 Tong, J.: Large nitrogen cycle perturbations during the Early Triassic hyperthermal, *Geochim.*  
515 *Cosmochim. Acta*, 382, 13–25, <https://doi.org/10.1016/j.gca.2024.08.009>, 2024.
- 516 Du, Y., Song, H., Algeo, T. J., Zhang, H., Peng, J., Wu, Y., Lai, J., Shu, X., Song, H., Wei, L., Zhang, J.,  
517 Stüeken, E. E., Grasby, S. E., Dal Corso, J., Dai, X., Chu, D., Tian, L., Liang, Q., Li, X., Yao, H.,  
518 and Song, H.: The global database of deep-time marine nitrogen isotope data [data set]. Zenodo.  
519 <https://doi.org/10.5281/zenodo.15117375>, 2025a.
- 520 Du, Y., Song, H., Algeo, T. J., Zhong, L., Li, J., and Song, H.: Tectonic controls on nitrogen cycling and  
521 ocean ventilation dynamics in the Late Cretaceous equatorial Atlantic, *Earth Planet. Sci. Lett.*, 667,  
522 119517, <https://doi.org/10.1016/j.epsl.2025.119517>, 2025b.
- 523 Farrell, Ú. C., Samawi, R., Anjanappa, S., Klykov, R., Adeboye, O. O., Agic, H., Ahm, A.-S. C., Boag,  
524 T. H., Bowyer, F., Brocks, J. J., Brunoir, T. N., Canfield, D. E., Chen, X., Cheng, M., Clarkson, M.  
525 O., Cole, D. B., Cordie, D. R., Crockford, P. W., Cui, H., Dahl, T. W., Mouro, L. D., Dewing, K.,  
526 Dornbos, S. Q., Drabon, N., Dumoulin, J. A., Emmings, J. F., Endriga, C. R., Fraser, T. A., Gaines,  
527 R. R., Gaschnig, R. M., Gibson, T. M., Gilleaudeau, G. J., Gill, B. C., Goldberg, K., Guilbaud, R.,  
528 Halverson, G. P., Hammarlund, E. U., Hantsoo, K. G., Henderson, M. A., Hodgskiss, M. S. W.,  
529 Horner, T. J., Husson, J. M., Johnson, B., Kabanov, P., Brenhin Keller, C., Kimmig, J., Kipp, M.  
530 A., Knoll, A. H., Kreitsmann, T., Kunzmann, M., Kurzweil, F., LeRoy, M. A., Li, C., Lipp, A. G.,  
531 Loydell, D. K., Lu, X., Macdonald, F. A., Magnall, J. M., Mänd, K., Mehra, A., Melchin, M. J.,  
532 Miller, A. J., Mills, N. T., Mwinde, C. N., O’Connell, B., Och, L. M., Ossa Ossa, F., Pagès, A.,  
533 Paiste, K., Partin, C. A., Peters, S. E., Petrov, P., Playter, T. L., Plaza-Torres, S., Porter, S. M.,



- 534 Poulton, S. W., Pruss, S. B., Richoz, S., Ritzer, S. R., Rooney, A. D., Sahoo, S. K., Schoepfer, S.  
535 D., Sclafani, J. A., Shen, Y., Shorttle, O., Slotznick, S. P., Smith, E. F., Spinks, S., Stockey, R. G.,  
536 Strauss, J. V., Stüeken, E. E., Tecklenburg, S., Thomson, D., Tosca, N. J., Uhlein, G. J., Vizcaíno,  
537 M. N., Wang, H., White, T., Wilby, P. R., et al.: The Sedimentary Geochemistry and  
538 Paleoenvironments Project, *Geobiology*, 19, 545–556, <https://doi.org/10.1111/gbi.12462>, 2021.
- 539 Gard, M., Hasterok, D., and Halpin, J. A.: Global whole-rock geochemical database compilation, *Earth*  
540 *Syst. Sci. Data*, 11, 1553–1566, <https://doi.org/10.5194/essd-11-1553-2019>, 2019.
- 541 Hendricks, G., Tkaczyk, D., Lin, J., and Feeney, P.: Crossref: The sustainable source of  
542 community-owned scholarly metadata, *Quant. Sci. Stud.*, 1, 414–427,  
543 [https://doi.org/10.1162/qss\\_a\\_00022](https://doi.org/10.1162/qss_a_00022), 2020.
- 544 Hoefs, J.: *Stable Isotope Geochemistry*, Springer International Publishing, Berlin,  
545 <https://doi.org/10.1007/978-3-030-77692-3>, 2021.
- 546 Ishida, A., Hashizume, K., and Kakegawa, T.: Microbial nitrogen cycle enhanced by continental input  
547 recorded in the Gunflint Formation, *Geochem. Persp. Lett.*, 13–18,  
548 <https://doi.org/10.7185/geochemlet.1729>, 2017.
- 549 Jenkyns, H. C.: Geochemistry of oceanic anoxic events, *Geochem. Geophys. Geosyst.*, 11, Q03004,  
550 <https://doi.org/10.1029/2009GC002788>, 2010.
- 551 Junium, C. K., Meyers, S. R., and Arthur, M. A.: Nitrogen cycle dynamics in the Late Cretaceous  
552 Greenhouse, *Earth Planet. Sci. Lett.*, 481, 404–411, <https://doi.org/10.1016/j.epsl.2017.10.006>,  
553 2018.
- 554 Kipp, M. A., Stüeken, E. E., Yun, M., Bekker, A., and Buick, R.: Pervasive aerobic nitrogen cycling in  
555 the surface ocean across the Paleoproterozoic Era, *Earth Planet. Sci. Lett.*, 500, 117–126,  
556 <https://doi.org/10.1016/j.epsl.2018.08.007>, 2018.
- 557 Knies, J., Grasby, S. E., Beauchamp, B., and Schubert, C. J.: Water mass denitrification during the  
558 latest Permian extinction in the Sverdrup Basin, Arctic Canada, *Geology*, 41, 167–170,  
559 <https://doi.org/10.1130/G33816.1>, 2013.
- 560 Kocsis, Á. T. and Scotese, C. R.: Mapping paleocoastlines and continental flooding during the  
561 Phanerozoic, *Earth Sci. Rev.*, 213, 103463, <https://doi.org/10.1016/j.earscirev.2020.103463>, 2021.
- 562 Koehler, M. C., Stüeken, E. E., Hillier, S., and Prave, A. R.: Limitation of fixed nitrogen and deepening  
563 of the carbonate-compensation depth through the Hirnantian at Dob’s Linn, Scotland, *Palaeogeogr.*  
564 *Palaeoclimatol. Palaeoecol.*, 534, 109321, <https://doi.org/10.1016/j.palaeo.2019.109321>, 2019.



- 565 Lai, J., Song, H., Chu, D., Dal Corso, J., Sperling, E. A., Wu, Y., Liu, X., Wei, L., Li, M., Song, H., Du,  
566 Y., Jia, E., Feng, Y., Song, H., Yu, W., Liang, Q., Li, X., and Yao, H.: Deep-Time Marine  
567 Sedimentary Element Database, *Earth Syst. Sci. Data*, 17, 1613–1626,  
568 <https://doi.org/10.5194/essd-17-1613-2025>, 2025.
- 569 Li, J., Song, H., Du, Y., Wignall, P. B., Bond, D. P. G., Grasby, S. E., Song, H., Dal Corso, J., Tian, L.,  
570 and Chu, D.: Spatial and temporal heterogeneity of the marine nitrogen cycle during the  
571 end-Triassic mass extinction, *Chem. Geol.*, 682, 122752,  
572 <https://doi.org/10.1016/j.chemgeo.2025.122752>, 2025.
- 573 Li, W., Zhou, L., Lin, Y., Zhang, H., Zhang, Y., Wu, X., Stevens, C., Yang, Y., Wang, H., Fang, Y., and  
574 Liang, F.: Interdisciplinary study on dietary complexity in Central China during the Longshan  
575 Period (4.5–3.8 kaBP): New isotopic evidence from Wadian and Haojiatai, Henan Province, *The  
576 Holocene*, 31, 258–270, <https://doi.org/10.1177/0959683620970252>, 2021.
- 577 Liu, Y., Magnall, J. M., Gleeson, S. A., Bowyer, F., Poulton, S. W., and Zhang, J.: Spatio-temporal  
578 evolution of ocean redox and nitrogen cycling in the early Cambrian Yangtze ocean, *Chem. Geol.*,  
579 554, 119803, <https://doi.org/10.1016/j.chemgeo.2020.119803>, 2020.
- 580 Liu, Z., Altabet, M. A., and Herbert, T. D.: Plio-Pleistocene denitrification in the eastern tropical North  
581 Pacific: Intensification at 2.1 Ma, *Chem. Geol.*, 9, 2008GC002044,  
582 <https://doi.org/10.1029/2008GC002044>, 2008.
- 583 Meyers, P. A., Yum, J.-G., and Wise, S. W.: Origins and maturity of organic matter in mid-Cretaceous  
584 black shales from ODP Site 1138 on the Kerguelen Plateau, *Mar. Pet. Geol.*, 26, 909–915,  
585 <https://doi.org/10.1016/j.marpetgeo.2008.09.003>, 2009.
- 586 Moretti, S., Auderset, A., Deutsch, C., Schmitz, R., Gerber, L., Thomas, E., Luciani, V., Petrizzo, M. R.,  
587 Schiebel, R., Tripathi, A., Sexton, P., Norris, R., D’Onofrio, R., Zachos, J., Sigman, D. M., Haug, G.  
588 H., and Martínez-García, A.: Oxygen rise in the tropical upper ocean during the Paleocene-Eocene  
589 Thermal Maximum, *Science*, 383, 727–731, <https://doi.org/10.1126/science.adh4893>, 2024.
- 590 Murphy, E. M. A. and Salvador, A.: International Subcommission on Stratigraphic Classification of  
591 IUGS International Commission on Stratigraphy, *Episodes*, 22, 1999.
- 592 National Research Council: *Scientific Ocean Drilling: Accomplishments and Challenges*, National  
593 Academies Press, Washington, D.C., <https://doi.org/10.17226/13232>, 2011.
- 594 Nichols, G.: *Sedimentology and stratigraphy*, John Wiley & Sons, 2009.
- 595 Pellerin, A., Thomazo, C., Ader, M., Rossignol, C., Rego, E. S., Busigny, V., and Philippot, P.:



- 596 Neoproterozoic oxygen-based nitrogen cycle en route to the Great Oxidation Event, *Nature*,  
597 <https://doi.org/10.1038/s41586-024-07842-x>, 2024.
- 598 Percival, L. M. E., Marynowski, L., Baudin, F., Goderis, S., De Vleeschouwer, D., Rakociński, M.,  
599 Narkiewicz, K., Corradini, C., Da Silva, A. -C., and Claeys, P.: Combined Nitrogen-Isotope and  
600 Cyclostratigraphy Evidence for Temporal and Spatial Variability in Frasnian–Famennian  
601 Environmental Change, *Geochem. Geophys. Geosyst.*, 23, e2021GC010308,  
602 <https://doi.org/10.1029/2021GC010308>, 2022.
- 603 Peters, K. E.: Guidelines for Evaluating Petroleum Source Rock Using Programmed Pyrolysis, *AAPG*  
604 *Bull.*, 70, 318–329, 1986.
- 605 Poulton, S. W. and Canfield, D. E.: Development of a sequential extraction procedure for iron:  
606 implications for iron partitioning in continentally derived particulates, *Chem. Geol.*, 214, 209–221,  
607 <https://doi.org/10.1016/j.chemgeo.2004.09.003>, 2005.
- 608 Sahoo, S. K., Gilleaudeau, G. J., Wilson, K., Hart, B., Barnes, B. D., Faison, T., Bowman, A. R.,  
609 Larson, T. E., and Kaufman, A. J.: Basin-scale reconstruction of euxinia and Late Devonian mass  
610 extinctions, *Nature*, 615, 640–645, <https://doi.org/10.1038/s41586-023-05716-2>, 2023.
- 611 Scotese, C.: The PALEOMAP Project PaleoAtlas for ArcGIS, version 1, 2, 16–31, ResearchGate [data  
612 set]. <https://doi.org/10.13140/RG.2.1.2011.4162>, 2008.
- 613 Scotese, C. R. and Wright, N.: PALEOMAP Paleodigital Elevation Models (PaleoDEMS) for the  
614 Phanerozoic PALEOMAP Project,  
615 <https://www.earthbyte.org/paleodem-resource-scotese-and-wright-2018/> (last access: 1 April  
616 2025), 2018.
- 617 Song, H.Y., Xing, T., Stüeken, E. E., Du, Y., Zhu, Y., Tao, X., Ni, Q., and Song, H.J.: Isotopic  
618 differences and paleoenvironmental significance of nitrogen contained in bulk sedimentary rocks,  
619 decarbonated aliquots and kerogen extracts, *Chem. Geol.*, 631, 121522,  
620 <https://doi.org/10.1016/j.chemgeo.2023.121522>, 2023.
- 621 Stüeken, E. E., Kipp, M. A., Koehler, M. C., and Buick, R.: The evolution of Earth’s biogeochemical  
622 nitrogen cycle, *Earth Sci. Rev.*, 160, 220–239, <https://doi.org/10.1016/j.earscirev.2016.07.007>,  
623 2016.
- 624 Stüeken, E. E., Pellerin, A., Thomazo, C., Johnson, B. W., Duncanson, S., and Schoepfer, S. D.: Marine  
625 biogeochemical nitrogen cycling through Earth’s history, *Nat. Rev. Earth Environ.*,  
626 <https://doi.org/10.1038/s43017-024-00591-5>, 2024.



- 627 Sun, Y.: Dynamics of nutrient cycles in the Permian–Triassic oceans, *Earth Sci. Rev.*, 258, 104914,  
628 <https://doi.org/10.1016/j.earscirev.2024.104914>, 2024.
- 629 Tesdal, J.-E., Galbraith, E. D., and Kienast, M.: Nitrogen isotopes in bulk marine sediment: linking  
630 seafloor observations with subseafloor records, *Biogeosciences*, 10, 101–118,  
631 <https://doi.org/10.5194/bg-10-101-2013>, 2013.
- 632 Thomazo, C., Ader, M., and Philippot, P.: Extreme 15 N-enrichments in 2.72-Gyr-old sediments:  
633 evidence for a turning point in the nitrogen cycle, *Geobiology*, 9, 107–120,  
634 <https://doi.org/10.1111/j.1472-4669.2011.00271.x>, 2011.
- 635 Tribouillard, N., Algeo, T. J., Lyons, T., and Riboulleau, A.: Trace metals as paleoredox and  
636 paleoproductivity proxies: An update, *Chem. Geol.*, 232, 12–32,  
637 <https://doi.org/10.1016/j.chemgeo.2006.02.012>, 2006.
- 638 Tucker, M. E. and Wright, V. P.: *Carbonate sedimentology*, John Wiley & Sons, 2009.
- 639 Uveges, B. T., Izon, G., Junium, C. K., Ono, S., and Summons, R. E.: Aerobic nitrogen cycle 100 My  
640 before permanent atmospheric oxygenation, *Proc. Natl. Acad. Sci.*, 122, e2423481122,  
641 <https://doi.org/10.1073/pnas.2423481122>, 2025.
- 642 Wang, D., Ling, H.-F., Struck, U., Zhu, X.-K., Zhu, M., He, T., Yang, B., Gamper, A., and Shields, G.  
643 A.: Coupling of ocean redox and animal evolution during the Ediacaran-Cambrian transition, *Nat.*  
644 *Commun.*, 9, 2575, <https://doi.org/10.1038/s41467-018-04980-5>, 2018.
- 645 Wilkinson, M. D., Dumontier, M., Sansone, S.-A., Bonino Da Silva Santos, L. O., Prieto, M., Batista,  
646 D., McQuilton, P., Kuhn, T., Rocca-Serra, P., Crosas, M., and Schultes, E.: Evaluating FAIR  
647 maturity through a scalable, automated, community-governed framework, *Sci. Data*, 6, 174,  
648 <https://doi.org/10.1038/s41597-019-0184-5>, 2019.
- 649 Winter, J. D.: *Principles of igneous and metamorphic petrology*, Pearson education Harlow, UK, 2014.
- 650 Xia, L., Cao, J., Stüeken, E. E., Hu, W., and Zhi, D.: Linkages between nitrogen cycling, nitrogen  
651 isotopes, and environmental properties in paleo-lake basins, *GSA Bull.*, 134, 2359–2372,  
652 <https://doi.org/10.1130/B36290.1>, 2022.
- 653 Zhong, L., Peng, J., He, J., Du, Y., Xing, T., Li, J., Guo, W., Ni, Q., Hu, J., and Song, H.: Optimizations  
654 of the EA-IRMS system for  $\delta^{15}\text{N}$  analysis of trace nitrogen, *Appl. Geochem.*, 159, 105832,  
655 <https://doi.org/10.1016/j.apgeochem.2023.105832>, 2023.